Extending the Depth-of-Field of Computational Ghost Imaging: Computational Refocus via in-situ Point Spread Function Estimation

Mengchao Ma,[1] Wenbo Liang,[1] Fushun Qin,[1] Qingtian Guan,[1] Xiang Zhong,[1] Huaxia Deng,[2] and Ziwei Wang[3]
[1)]*Anhui Province Key Laboratory of Measuring Theory and Precision Instrument, School of Instrument Science and Opto-Electronics Engineering, Hefei University of Technology, Hefei, 230009, China*
[2)]*CAS Key Laboratory of Mechanical Behavior and Design of Materials, Department of Modern Mechanics, University of Science and Technology of China, Hefei, Anhui 230027, China.*
[3)]*School of Engineering, Lancaster University, Lancaster, LA1 4YW, United Kingdom*

(*Electronic mail: zhx0325@hfut.edu.cn; hxdeng@ustc.edu.cn.)

(Dated: 20 December 2023)

Capturing details of objects beyond the focal plane is challenging due to the limited Depth-of-Field (DoF) of optical systems. Here, we report a Computational Refocusing Ghost Imaging (CRGI) method to extend the DoF of computational ghost imaging (CGI) systems. An ultra-fast and in-situ Point Spread Function (PSF) estimation method is put forward utilizing the optical characterization of the system and compressive sensing (CS) modulation. The PSF distribution is measured with in-situ compressive sensing algorithm according to reciprocity property using the same CGI system. The convolution of PSFs of various depths with modulation patterns is reshaped into measurement matrices to computationally refocus objects at different depths. From one measurement, CRGI can rebuild distinct and well-focused images of multiple objects at different depths. According to experiments, CRGI can nearly quadruple the DoF of typical CGI methods. CRGI represents a significant advancement in CGI domain by computationally surpassing the optical DoF limitations. This discovery enables recording object features beyond the focus plane using Extended Depth-of-Field (EDoF).

Achieving accurate object details beyond the focal plane is challenging due to DoF limitations in optical imaging. Conventional cameras typically achieve EDoF by capturing multiple images at different focal lengths and then fusing them into a full-focus image[1]. In contrast, computational ghost imaging (CGI)[2–4] uses structured illumination and a non-spatially resolved single-point detector (SPD) to collect reflected light signals and create an image. Since CGI does not rely on arrayed sensors, it excels in non-visible wavelengths[5–8] and extreme conditions[9–11], making it adaptable to a variety of scenarios such as microscopic imaging[12], liveness detection[13], and 3D imaging[14–16]. However, the imaging DoF of CGI is also constrained to the projection lens because it uses projector-focused structural illumination. The focal length of the projection lens must be adjusted multiple times and a large number of illumination patterns projected to merge multi-focus images at different depths for CGI, which is time-consuming and cumbersome.

To enable sharp imaging in areas beyond the focal length of the projection lens, Xu et al.[17] proposed a projector defocus correction method for Fourier single-pixel imaging. However, it relies on prior knowledge of the focus location and uses an additional camera to obtain focus patterns. Rizvi et al.[18] introduced a deep learning neural network-based technique for defocus compensation, but it necessitates extensive data preparation and training, particularly when modulation changes. Toninelli et al.[19] validated the use of caustic patterns as the basis for single-pixel imaging of objects at distances ranging from 3 cm to 15 cm. Qi et al.[20] presented an active autofocusing solution for projectors that eliminates manual focusing, but it fails to overcome the DoF constraint. Moreover, these methods can only refocus a non-focal plane in a single measurement, making the acquisition of a collection of multi-focus images equally time-consuming.

In this letter, we present a Computational Refocusing Ghost Imaging (CRGI) method for EDoF of CGI systems via in-situ PSF measurements. The process involves PSFs convolution with original modulation patterns across a range of depths. To obtain the PSF, we present a quick, in-situ PSF measurement method for the CGI system. PSF calibration is done only once, and then we can refocus on targets at varied depths and positions allowing sharp imaging of multi-focus objects.

Point Spread Function is an optical system's impulse response to a point light source. However, it's a surface illumination from a projector for the CGI setup. According to the theory of light propagation, although the PSF of an optical system can be obtained through computational methods such as mathematical modeling and software simulation, accurately calculating the PSF through these methods poses challenges due to various factors like noise, aberrations from imperfect lenses, and the need for prior knowledge. Deviations between the simulated PSF and the system can result in failed recovery. Additionally, obtaining the PSF through calculation is difficult for certain devices used in practice. It has been demonstrated that PSF of an optical system can be measured based on the idea of ghost imaging. Li et al.[21] proposed to obtain the PSF of the diffuser by calculating the spatial correlation between the results of two cameras, with which imaging beyond a single memory effect range can be achieved, through scattering layers. This approach can easily and efficiently acquire PSFs with spatial variations. However, for CGI systems, using SPD that are not spatially resolved to acquire PSF gives them an advantage in the non-visible wavelength band. So in accordance with reciprocity between CGI systems and conventional cameras, we propose a method to measure the PSF of a specific CGI imaging sys-

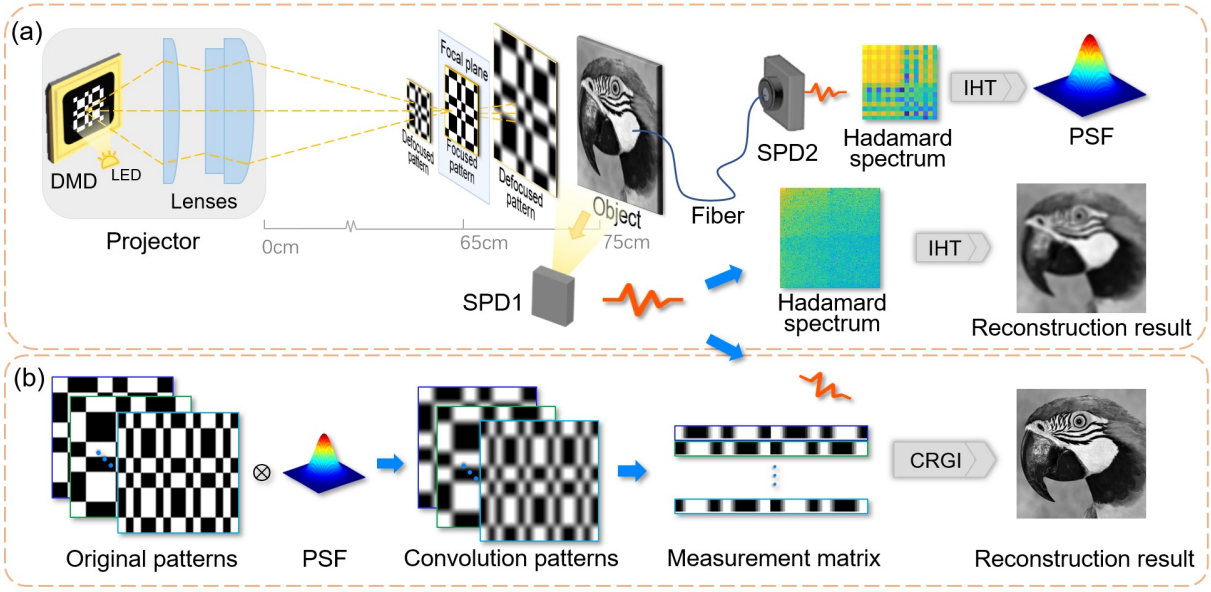

FIG. 1. Illustration of the proposed CRGI method. (a) Schematic diagram of the experimental setup. The object is placed in a non-focal position. The fiber end face is located at the same position as the object for PSF estimation. Blurred image reconstructed by inverse Hadamard transforms (IHT). (b) The reconstruction process of the proposed CRGI method.

tem by coupling an SPD to a fiber and calculating the in-situ distribution of the PSF with a well-developed SPI technique such as Hadamard Single-pixel Imaging (HSI)[22]. Basically, the method doesn't need to alter between the imaging mode and the PSF measuring mode, hence the in-situ nomenclature. After obtaining the PSF, the actual illumination paradigm due to defocus at varying object distances can be estimated by applying the PSF as a convolutional kernel to the original illumination patterns. Eventually, a sharp focused imaging result can be obtained by correlation between the refined patterns and SPD measurements.

As shown in Fig.1(a), CGI typically comprises an object modulation and image reconstruction process. When the object is situated out of DoF during the modulation process, the measured SPD data is distorted due to defocusing. Directly applying conventional reconstruction approaches (such as Inverse Hadamard Transform) will result in blurring of the rebuilt image. CS[23] is an alternate reconstruction technique that could fix the defocusing flaw. Generally, the CS takes correlation between the modulation patterns (which are reshaped into a measurement matrix) and the measurement data for image reconstruction. However, when modulations are out-of-focus, directly applying standard CS algorithm still results in blurred images.

In this contribution, to achieve computational refocusing for objects beyond the focal plane, CRGI was developed to retrieve the best estimation of the defocused modulation patterns via convolution. This estimation is then reshaped as refined measurement matrix inputs to coincide with the actual projected defocused patterns for image reconstruction, as shown in Fig. 1(b). Specifically, the setup shown in Fig. 1(a) is used to acquire PSFs at different depths. In conventional imaging systems, the camera acquires PSF by directly photographing a point light source. According to Helmholtz reciprocity[24], the projector and SPD are equivalent to the camera and light source, respectively. Therefore, the PSF can be obtained directly with standard CGI procedures. However, the SPD is not equivalent to a point light source due to its bulky light-sensitive area. So, we couple the SPD with an optical fiber so that its sensing area is only the size of the fiber's end face and is equivalent to a point light source. In the experiments, we used a multimode fiber with an operating band from 200 nm to 1200 nm, a core diameter of 300 μm, and a length of about 1 meter. The end face of the fiber can be considered as a pinhole through which light is transmitted to the SPD. In addition, the PSF distribution is rather condensed and tends to have a very small size. Low-resolution modulation patterns (e.g., Hadamard basis patterns with a 16×16-pixel resolution and a quantity of $16 \times 16 \times 2$.) are sufficient for a fairly good PSF estimation (see Supplementary Material for more details). This allows us to efficiently estimate the PSFs at different depths in the CGI system. Although PSFs must be calibrated at various depths, this process takes an extremely short time and only needs to be done once. The acquired PSFs can be reused without re-calibration.

The CRGI approach is very scalable and compatible with many illumination patterns, such as random[2], Fourier[25] and Hadamard[22] (see Supplementary Material for results using random and Fourier patterns). In this work, Hadamard basis patterns were adopted without losing generality, taking into consideration their orthogonality and binary character. The Hadamard basis patterns $P(x,y)$ are derived from the Hadamard matrix[22]. As depicted in Fig.1(a), defocusing occurs when patterns are projected onto an object distant from the focal plane. The PSF of the optical device can be modeled as a circular Gaussian filter, as shown in Fig.1(b). Thus

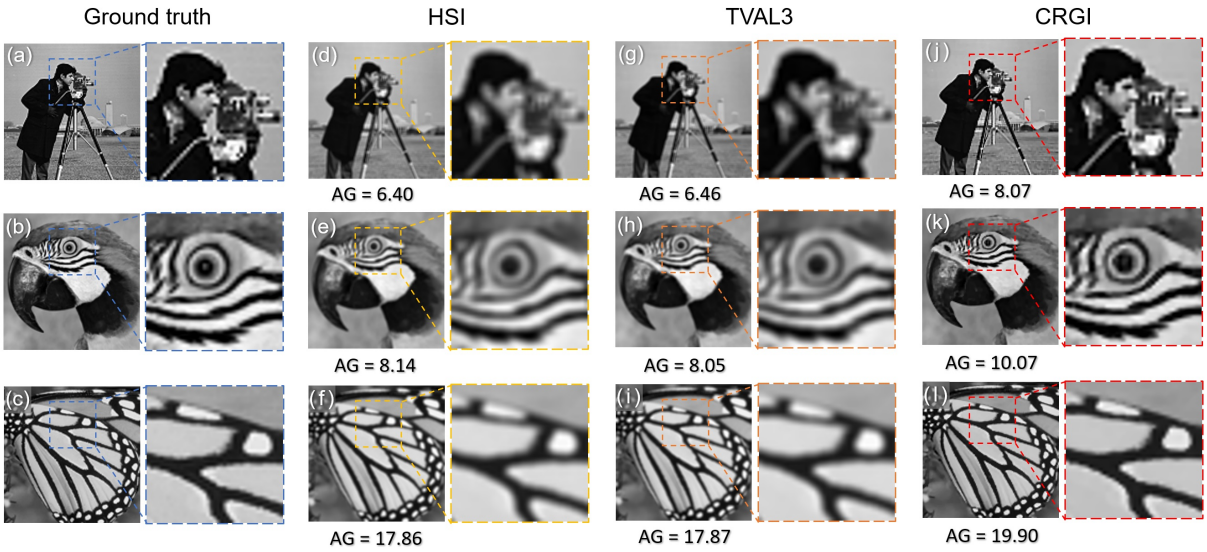

FIG. 2. Comparison of simulation results with defocus modulations. Partial enlargements and AG values are also given together. (a)-(c) Ground truth. (d)-(f) Reconstructed images with HSI. (g)-(i) Reconstructed images with TVAL3. (j)-(l) Reconstructed images with the proposed CRGI method.

the defocused modulation pattern $P^{'}(x,y)$ can be expressed as the convolution of original pattern $P(x,y)$ with the PSF kernel $G(x,y;\sigma)$:

$$P^{'}(x,y) = P(x,y) \otimes G(x,y;\sigma) \tag{1}$$

$$G(x,y;\sigma) = \frac{1}{2\pi\sigma^2} \exp(-\frac{x^2+y^2}{2\sigma^2}) \tag{2}$$

In practice, $G(x,y;\sigma)$ is measured by in-situ CGI method. $\otimes$ denotes the convolution operation. σ is the standard deviation used to adjust the ambiguity distribution, and (x,y) is the spatial coordinate.

When the object is placed at the non-focal plane, N modulation patterns are $P^{'} = \left\{P_1^{'}, P_2^{'}, P_3^{'}, \ldots, P_N^{'}\right\}$. Then the SPD detection intensity B_n corresponding to the n-th modulation pattern is

$$B_n = \sum_{x=0}^{N-1}\sum_{y=0}^{N-1} P_n^{'}(x,y) \cdot I(x,y) \tag{3}$$

where $I(x,y)$ is the distribution function of the object. For the CGI with CS reconstruction, the vector form of Eq. 3 can be expressed as

$$\mathbf{B} = \mathbf{A}^{'}\mathbf{I} \tag{4}$$

where $\mathbf{B}$ and $\mathbf{I}$ are the vectorized representations of a series of B_n and $I(x,y)$, respectively. $\mathbf{A}^{'}$ is a measurement matrix consisting of all of the defocused modulation patterns $P^{'}$, and the n-th row of $\mathbf{A}^{'}$ is the vectorized form of $P_n^{'}$.

Numerous optimization techniques have been developed to rebuild image $\mathbf{I}$ from incomplete observations $\mathbf{B}$, among which the TVAL3[26] is widely used for its excellent solving performance and was adopted as the reconstruction method for the proposed CRGI method in this paper. Although TVAL3 is usually used for compressed sampling reconstruction, compressed sampling usually results in blurring of the reconstructed image. To avoid the effect of compressive sampling, the sampling rate was set at 1 in all simulations and experiments.

Figure 2 depicts a comparison of simulation results when defocusing modulations are present. According to Eq.(1) and Eq.(2), a Gaussian filter of size 3×3 and $\sigma = 1.5$ was used as the defocusing blur kernel (i.e. PSF). The convolution results of the original Hadamard basis patterns with the PSF kernel were then used as the projected patterns to emulate the defocusing of the modulation patterns. To objectively evaluate the sharpness of the simulation results, we use the sharpness evaluation metric Average Gradient (AG)[27] to quantify the sharp-

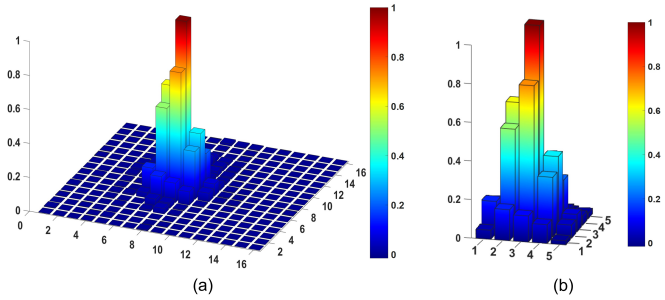

FIG. 3. Experimentally acquired PSF. (a) The normalized PSF of 16 × 16-pixel resolution by CRGI. (b) The PSF of 5 × 5-pixel resolution is derived by clipping the region centered around the maximum pixel values in (a).

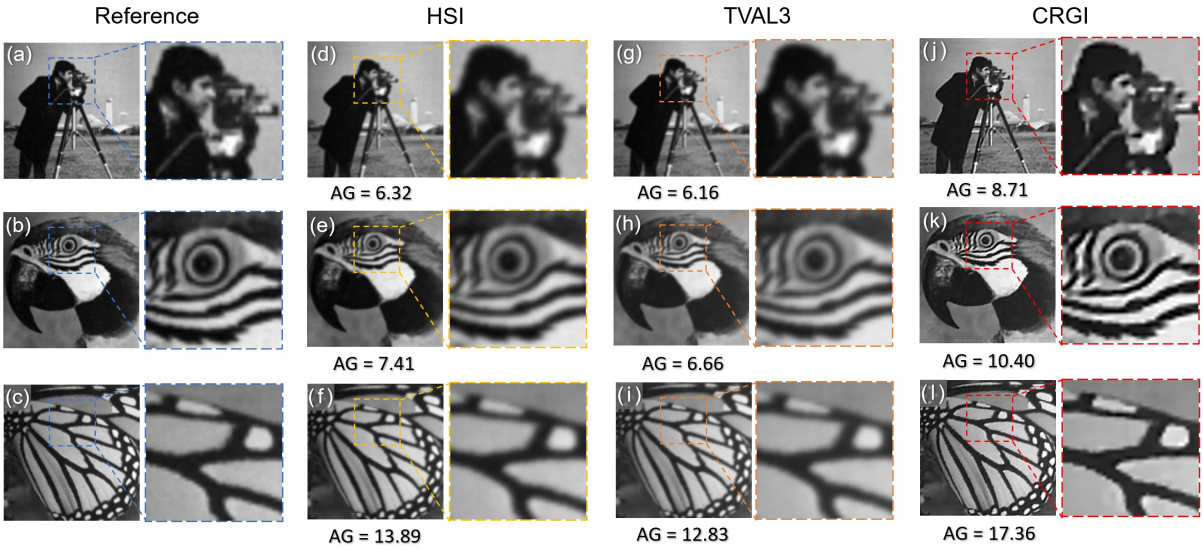

FIG. 4. Comparison of experimental results. (a)-(c) Reference. (d)-(f) Reconstructed images of out-of-focus objects with HSI. (g)-(i) Reconstructed images of out-of-focus objects with TVAL3. (j)-(l) Reconstructed images of out-of-focus objects with proposed CRGI method

ness,

$$AG = \frac{1}{M \times N} \sum_{i=1}^{M} \sum_{j=1}^{N} \sqrt{\frac{(\frac{\partial I(x,y)}{\partial x})^2 + (\frac{\partial I(x,y)}{\partial y})^2}{2}} \tag{5}$$

where $M \times N$ is the resolution of the image $I(x,y)$. $\frac{\partial I(x,y)}{\partial x}$ and $\frac{\partial I(x,y)}{\partial y}$ denote the gradient in the horizontal and vertical directions of the image, respectively. Higher AG values indicate higher image sharpness.

Cameraman, Parrot, and Butterfly images with 128×128-pixel resolution are used as targets. The first column of Fig.2 presents the ground truth. The second column gives HSI reconstruction outcomes using IHT directly. The third column shows reconstructed images by directly applying TVAL3 with original Hadamard patterns as the measurement matrix. Due to defocusing, both the SPD measurements and measurement matrix are corrupted, causing apparent image blur in Fig.2(d)–(i). The last column shows the reconstructed images with the proposed CRGI method. It produces sharp images that are almost identical to the ground truths. The results in Fig. 2 were further quantitatively evaluated with AG values, which also indicate that CRGI reconstructs images better than HSI and TVAL3.

The first experiment verified the CRGI method's practicality. See the experimental scheme in Fig. 1. The DLP projector (V7001) was used to cast Hadamard patterns onto the objects. The data acquisition board receives electrical signals from the SPD (PDA100A2) based on the intensity of the reflected light. The object was 75 cm away from the projector. Since the projector lenses were adjusted to a focal length of around 65 cm, the object is 10 cm out-of-focus. To precisely measure the PSF, the fiber end faces the projector and is placed in the same position as the object. Hadamard basis patterns with notably low resolution of 16×16 pixels are sufficient to illuminate the fiber end faces to get a fairly accurate estimation of the PSF through standard HSI algorithm. The PSF measuring setup is identical to the imaging setup without changing the SPD position. This configuration characterizes the proposed CRGI method as an in-situ approach, enabling rapid acquisition of PSF data.

The experimentally measured PSF is illustrated in Fig. 3(a). Notably, the values are concentrated in the central zone and drop sharply outwards. Thus, a 5×5-pixel sub-region is cropped as the PSF kernel, as shown in Fig. 3(b). this kernel is subsequently convoluted with the original Hadamard basis patterns to create an amended measurement matrix to facilitate the reconstruction of clear images. The measured PSF was utilized to reconstruct images with the proposed CRGI method and compared with HSI and TVAL3 methods. The experimental results are shown in Fig. 4, where we use the HSI reconstructed images of objects located at the focal plane as reference. Intuitive perception of the experimental results shows that the reconstructed images using the CRGI method are almost identical to the reference images. Compared with HSI and TVAL3 results, the CRGI reconstructions are sharper and show more details. The suggested method greatly outperforms the other two methods, with an improvement of nearly 50% in terms of AG values. This is consistent with human intuitive perception.

We further demonstrate the computational refocusing capability of the proposed CRGI method in multi-depth 3D scenes. The experimental setup is shown in Fig.5. The focal length of the projector lenses was set to be 70 cm. Objects 1 and 3 were situated 60 cm and 85 cm from the projector, respectively. To achieve computational refocusing imaging of objects at different depths, PSFs at the same multiple depths need to be measured. The measurement setup is shown in Fig. 5 (b), where a series of low-resolution Hadamard patterns are projected onto the fiber end face, the light is transmitted to the

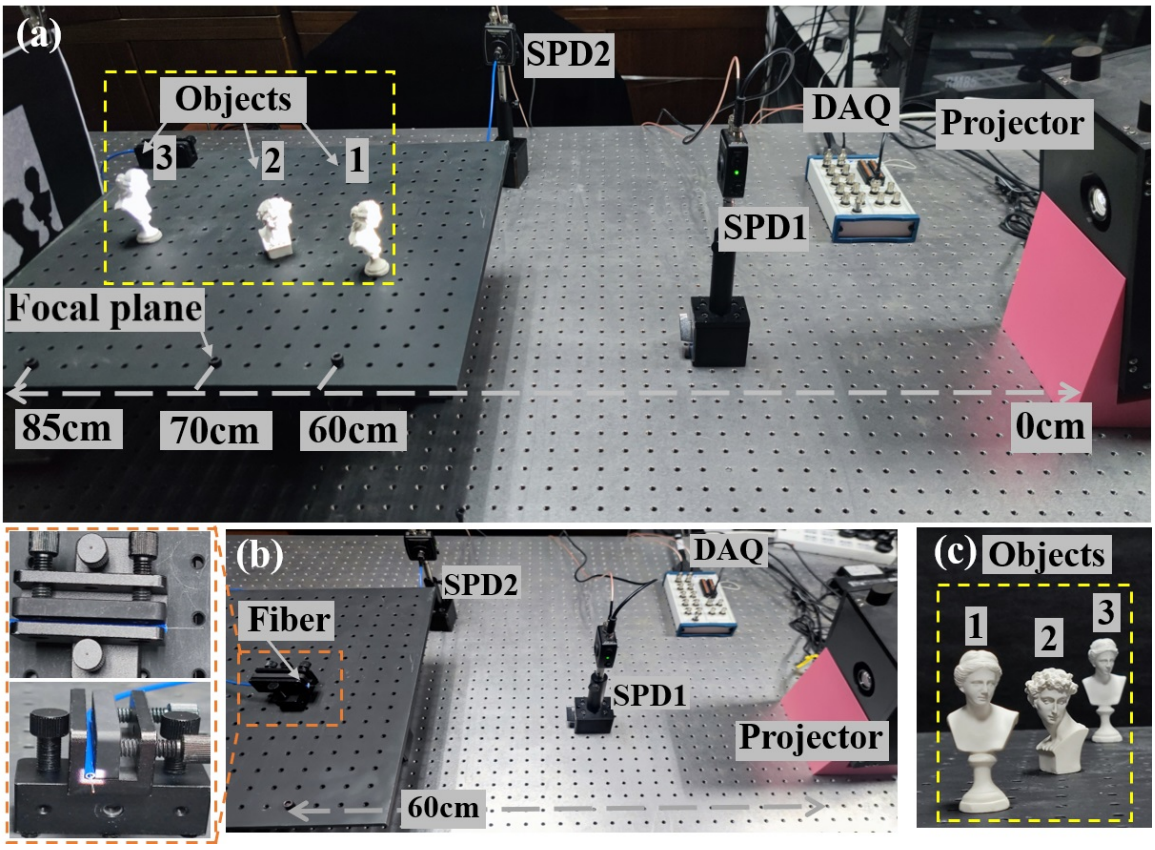

FIG. 5. EDoF experimental setup. (a) Multi-depth 3D experimental scene. Objects 1 and 3 are in the non-focal plane and object 2 is in the focal plane. (b) Experimental setup for PSF measurement. Only the PSF measurement at object 1 is shown. (c) Front view of objects 1, 2, and 3 in (a). SPD: single point detector. DAQ: data acquisition board. The system DoF is 2.5 cm. See supplementary material for simultaneous PSF measurements and imaging, and the spatial resolution of the system.

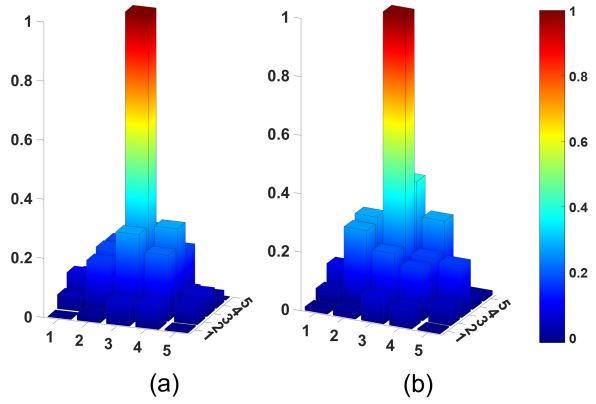

FIG. 6. PSFs estimation for positions of object 1 and object 3. (a) PSF at object 1 position. (b) PSF at object 3 position.

SPD2 through fiber to be converted into electrical signals, and the PSFs are obtained by the HSI algorithm. Fig. 6 shows the PSFs measured in the experiment located at objects 1 and 3. In the imaging process, the projector cast 128×128-pixel Hadamard patterns onto the objects. The reflected light intensity signal was captured by the SPD1 and subsequently sampled using the data acquisition board. Note that only a solitary data acquisition is performed. This data is utilized to perform computational refocusing on both objects 1 and 3, separately.

The experimental results of the multi-depth 3D scene are shown in Fig. 7. Because objects 1 and 3 are located out-of-focus, they exhibited blurred imaging results with the HSI method, as is shown in Fig. 7 (a). To extend the DoF of the system, we conducted computational refocusing on objects 1 and 3 individually. The PSFs in Fig. 6 (a) and (b) were convoluted with original Hadamard basis patterns, which were then reshaped into refined measurement matrices as input for the computational refocusing using CRGI for objects 1 and 3, respectively.

Figures 7 (b) and (c) show the images of objects 1 and 3 after computational refocusing, which are well-defined, clear, and highly detailed compared to FIG. 7 (a). Notably, when computational refocusing is performed on object 1 (or 3), object 3 (or 1) also becomes clear because these two locations have similar PSFs. Meanwhile, object 3 becomes blurred at this point, just like when using a camera with manual focusing or autofocusing adjustment. However, the proposed CRGI method refines a series of images with varying focus points by computational refocusing with only a single data acquisition procedure, eliminating the need to capture multiple images,

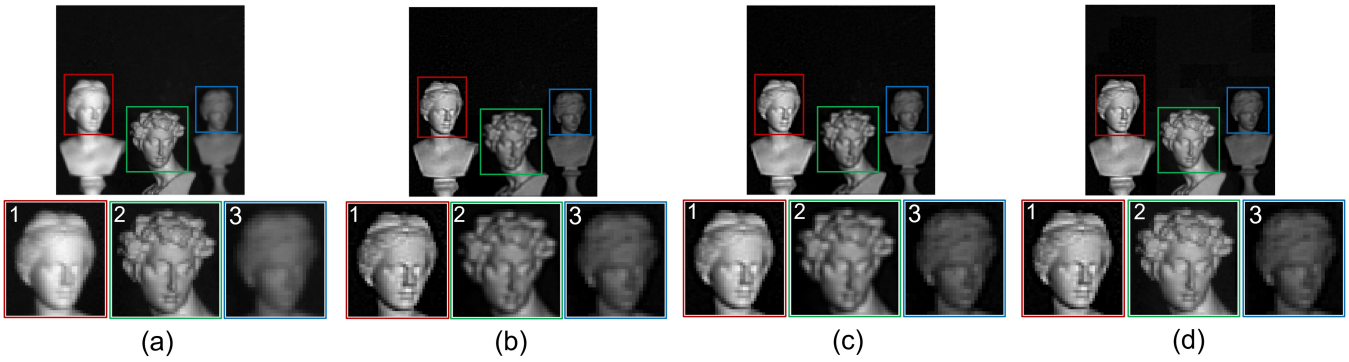

FIG. 7. Multi-depth computational refocusing experimental results. (a) Reconstruction result by HSI. (b) Reconstruction result of computational refocusing for object 1 by CRGI. (c) Reconstruction result of computational refocusing for object 3 by CRGI. (d) A full-focus image by image fusion of images (a), (b) and (c).

as required by post-imaging processing with a camera. Using the multi-focus image fusion technique based on variance in discrete cosine transform domain[28], a full-focus image of the 3D scene can be fused in Fig. 7 (d), utilizing in (a) and refocused images (b) and (c). In addition, we demonstrate the depth resolution of the CRGI method, which is detailed in the Supplementary Material.

Typically, to fuse images captured by a CCD/CMOS camera using image fusion techniques, image alignment[29] is necessary to ensure that the scenes and imaging conditions are consistent. Unfortunately, this can lead to longer processing times and may not always be feasible. On the contrary, the proposed CRGI approach is trouble free of any alignment prerequisites. It performs computational refocusing of objects at different depths all with only one data acquisition. Therefore, the imaging scenes and conditions of the different focus depths are identical without any image alignment. Our method is well-suited for multi-focus image fusion techniques, and it can effectively extend the Depth-of-Field of CGI systems.

In this letter, we propose an extended Depth-of-Field CGI method via in-situ PSF measurement of various depths. The convolution of PSFs with modulation patterns produces refined modulation patterns, which are then reshaped into measurement matrices for the computational refocusing of objects at different depths using CS reconstruction algorithms. Although measuring PSFs at varying depths is necessary, the suggested PSF measurement approach only requires a small number of modulation patterns with extremely low resolutions. This enables us to obtain the PSFs at different depths easily and quickly. Furthermore, PSF measurements with CRGI differ from cameras which rely on capturing images of a point light source. Instead, the differential operation during measurements can help to reduce noise, enhance the precision of PSFs, and be more compatible with CGI systems.

In single object out-of-focus experiment, the CRGI produces sharper images compared to conventional methods, both in terms of intuitive perception and AG values. In multi-depth 3D experimental scenes, CRGI enables computational refocusing imaging of objects at varying depths, even if they are at different non-focal planes. This can significantly extend the DoF of the imaging system. Furthermore, a full-focused image of the 3D scene via multi-focus image fusion can be achieved without requiring any image alignment. In 3D measurements, the use of sharper images leads to better measurements and greater DoF for 3D measurements[30,31]. In CGI-based 3D measurements[16], the CRGI can provide clear imaging and larger DoF, which facilitates the experimentation of 3D measurements with a large DoF.

In conclusion, CRGI effectively achieves EDoF for CGI systems, seamlessly integrating with diverse modulation patterns and CS reconstruction algorithms. Its straightforward implementation, efficiency, and adaptability make it a promising method for computational refocusing, with potential applications in EDoF optical microscopic imaging and beyond.

See the Supplementary Material for details of PSF estimation, discussion about the depth resolution of CRGI, results using random and Fourier basis patterns, simultaneous PSF measurements and imaging experiment, and spatial resolution of the system.

ACKNOWLEDGMENTS

This work is supported by National Natural Science Foundation of China (Grant No. 52275529 and 12372187), the Natural Science Foundation of Anhui Province (Grant No. 2208085ME138), the Fundamental Research Funds for the Central Universities (Grant Nos. WK2090000039 and WK2480000010), and the CAS Talent Introduction Program (No. KY2090000077).

AUTHOR DECLARATIONS

Conflict of Interest

The authors declare no conflicts of interest.

Author Contributions

Mengchao Ma: Conceptualization (equal); Funding acquisition (equal); Software (equal); Validation (equal); Visualization (equal); Writing - original draft (equal); Writing – review & editing (equal). **Wenbo Liang**: Conceptualization (equal); Software (equal); Validation (equal); Visualization (equal); Writing - original draft (equal); Writing – review & editing (equal). **Fushun Qin**: Validation (equal); Visualization (equal). **Qingtian Guan**: Validation (equal); Visualization (equal). **Xiang Zhong**: Funding acquisition (equal); Validation (supporting). **Huaxia Deng**: Conceptualization (equal); Funding acquisition (equal); Writing – original draft (equal); Writing – review & editing (equal). **Ziwei Wang**: Validation (equal); Writing – review & editing (equal).

DATA AVAILABILITY STATEMENT

The data that support the findings of this study are available from the corresponding author upon reasonable request.

REFERENCES

[1] Y. Liu, X. Chen, H. Peng, and Z. Wang, "Multi-focus image fusion with a deep convolutional neural network," Information Fusion **36**, 191–207 (2017).

[2] J. H. Shapiro, "Computational ghost imaging," Physical Review A **78** (2008), 10.1103/PhysRevA.78.061802.

[3] B. I. Erkmen and J. H. Shapiro, "Ghost imaging: from quantum to classical to computational," Advances in Optics and Photonics **2**, 405–450 (2010).

[4] F. Devaux, P.-A. Moreau, S. Denis, and E. Lantz, "Computational temporal ghost imaging," Optica **3**, 698–701 (2016).

[5] Y.-H. He, A.-X. Zhang, M.-F. Li, Y.-Y. Huang, B.-G. Quan, D.-Z. Li, L.-A. Wu, and L.-M. Chen, "High-resolution sub-sampling incoherent x-ray imaging with a single-pixel detector," APL Photonics **5** (2020), 10.1063/1.5140322.

[6] W. L. Chan, K. Charan, D. Takhar, K. F. Kelly, R. G. Baraniuk, and D. M. Mittleman, "A single-pixel terahertz imaging system based on compressed sensing," Applied Physics Letters **93** (2008), 10.1063/1.2989126.

[7] C. Zhao, W. Gong, M. Chen, E. Li, H. Wang, W. Xu, and S. Han, "Ghost imaging lidar via sparsity constraints," Applied Physics Letters **101** (2012), 10.1063/1.4757874.

[8] R. I. Stantchev, B. Sun, S. M. Hornett, P. A. Hobson, G. M. Gibson, M. J. Padgett, and E. Hendry, "Noninvasive, near-field terahertz imaging of hidden objects using a single-pixel detector," Science Advances **2** (2016), 10.1126/sciadv.1600190.

[9] D. Huyan, N. Lagrosas, and T. Shiina, "Target imaging in scattering media using ghost imaging optical coherence tomography," APL Photonics **7** (2022), 10.1063/5.0099638.

[10] M. Ma, Y. Zhang, H. Deng, X. Gao, L. Gu, Q. Sun, Y. Su, and X. Zhong, "Super-resolution and super-robust single-pixel superposition compound eye," Optics and Lasers in Engineering **146** (2021), 10.1016/j.optlaseng.2021.106699.

[11] M. Ma, W. Liang, X. Zhong, H. Deng, D. Shi, Y. Wang, and M. Xia, "Direct noise-resistant edge detection with edge-sensitive single-pixel imaging modulation," Intelligent Computing **2**, 0050 (2023), https://spj.science.org/doi/pdf/10.34133/icomputing.0050.

[12] A. Ghezzi, A. J. M. Lenz, F. Soldevila, E. Tajahuerce, V. Vurro, A. Bassi, G. Valentini, A. Farina, and C. D'Andrea, "Computational based time-resolved multispectral fluorescence microscopy," APL Photonics **8** (2023), 10.1063/5.0135452.

[13] Q. Guan, H. Deng, W. Liang, M. Ni, X. Gao, M. Ma, X. Zhong, and X. Gong, "Resolution-independent liveness detection via computational ghost imaging," Applied Physics Letters **123**, 021101 (2023), https://pubs.aip.org/aip/apl/article-pdf/doi/10.1063/5.0155365/18034824/021101_1_5.0155365.pdf.

[14] Y. Jie, X. Li, Z. Zhang, J. Wang, Y. Hu, Y. Li, W. He, and C. Zhao, "Three-dimensional imaging by compressed sensing based dual-frequency laser phase ranging," APL Photonics **8**, 076104 (2023), https://pubs.aip.org/aip/app/article-pdf/doi/10.1063/5.0152561/18033303/076104_1_5.0152561.pdf.

[15] C. A. Osorio Quero, D. Durini, J. Rangel-Magdaleno, and J. Martinez-Carranza, "Single-pixel imaging: An overview of different methods to be used for 3D space reconstruction in harsh environments," Review of Scientific Instruments **92** (2021), 10.1063/5.0050358.

[16] B. Sun, M. P. Edgar, R. Bowman, L. E. Vittert, S. Welsh, A. Bowman, and M. J. Padgett, "3D computational imaging with single-pixel detectors," Science **340**, 844–847 (2013).

[17] B. Xu, H. Jiang, H. Zhao, X. Li, and S. Zhu, "Projector-defocusing rectification for fourier single-pixel imaging," Optics Express **26**, 5005–5017 (2018).

[18] S. Rizvi, J. Cao, and Q. Hao, "Deep learning based projector defocus compensation in single-pixel imaging," Optics Express **28**, 25134–25148 (2020).

[19] E. Toninelli, D. Stellinga, B. Sephton, A. Forbes, and M. J. Padgett, "Single-pixel imaging using caustic patterns," Scientific Reports **10** (2020), 10.1038/s41598-020-59224-8.

[20] S. Qi, Z. Deng, P. Qi, J. Liao, Z. Zhang, G. Zheng, and J. Zhong, "Image-free active autofocusing with dual modulation and its application to fourier single-pixel imaging," Optics Letters **48**, 1970–1973 (2023).

[21] L. Li, Q. Li, S. Sun, H.-Z. Lin, W.-T. Liu, and P.-X. Chen, "Imaging through scattering layers exceeding memory effect range with spatial-correlation-achieved point-spread-function," Opt. Lett. **43**, 1670–1673 (2018).

[22] L. Wang and S. Zhao, "Fast reconstructed and high-quality ghost imaging with fast walsh-hadamard transform," Photonics Research **4**, 240–244 (2016).

[23] M. P. Edgar, G. M. Gibson, and M. J. Padgett, "Principles and prospects for single-pixel imaging," Nature Photonics **13**, 13–20 (2019).

[24] M. Born and E. Wolf, *Principles of Optics*, 7th ed. (Cambridge University Press, 2019).

[25] H. Deng, X. Gao, M. Ma, P. Yao, Q. Guan, X. Zhong, and J. Zhang, "Fourier single-pixel imaging using fewer illumination patterns," Applied Physics Letters **114** (2019), 10.1063/1.5097901.

[26] C. Li, W. Yin, H. Jiang, and Y. Zhang, "An efficient augmented lagrangian method with applications to total variation minimization," Computational Optimization and Applications **56**, 507–530 (2013).

[27] M. Zhu, L. Yu, Z. Wang, Z. Ke, and C. Zhi, "Review: A survey on objective evaluation of image sharpness," Applied Sciences-basel **13** (2023), 10.3390/app13042652.

[28] M. Naji and A. Aghagolzadeh, "A new multi-focus image fusion technique based on variance in dct domain," in *2015 2nd International Conference on Knowledge-Based Engineering and Innovation (KBEI). Proceedings* (2015) pp. 478–84, 2015 2nd International Conference on Knowledge-Based Engineering and Innovation (KBEI), 5-6 Nov. 2015, Tehran, Iran.

[29] X. Xia, G. Dang, Y. Yao, and J. Liang, "Image registration model and algorithm for multi-focus images," Pattern Recognition Letters **86**, 26–30 (2017).

[30] L. Chen and S. Zhang, "Large depth-of-field microscopic structured-light 3D imaging with focus stacking," OPTICS AND LASERS IN ENGINEERING **167** (2023), 10.1016/j.optlaseng.2023.107623.

[31] L. Chen, X. Hu, and S. Zhang, "Calibration method for an extended depth-of-field microscopic structured light system," OPTICS EXPRESS **30**, 166–178 (2022).